Effects of Arylene Diimide Thin Film Growth Conditions on n-Channel OFET Performance

ARTICLE *in* ADVANCED FUNCTIONAL MATERIALS · APRIL 2008

Impact Factor: 11.81 · DOI: 10.1002/adfm.200701045

ADVANCED FUNCTIONAL MATERIALS

DOI: 10.1002/adfm.200701045

Effects of Arylene Diimide Thin Film Growth Conditions on n-Channel OFET Performance**

By *Brooks A. Jones, Antonio Facchetti, Michael R. Wasielewski,** and *Tobin J. Marks**

A series of eight perylene diimide (PDI)- and naphthalene diimide (NDI)-based organic semiconductors was used to fabricate organic field-effect transistors (OFETs) on bare SiO_2 substrates, with the substrate temperature during film deposition (T_d) varied from 70–130 °C. For the *N,N′-n*-octyl materials that form highly ordered films, the mobility (μ) and current on-off ratio (I_{on}/I_{off}) increase slightly from 70 to 90 °C, and remain relatively constant between 90 and 130 °C. I_{on}/I_{off} and μ of dibromo-PDI-based OFETs decrease with increasing T_d, while films of *N,N′*-1*H*,1*H*-perfluorobutyl dicyanoperylenediimide (PDI-FCN_2) exhibit dramatic I_{on}/I_{off} and μ enhancements with increasing T_d. Increased OFET mobility can be correlated with higher levels of molecular ordering and minimization of film morphology surface irregularities. Additionally, the effects of SiO_2 surface modification with trimethylsilyl and octadecyltrichlorosilyl monolayers, as well as with polystyrene, are investigated for *N,N′-n*-octyl dicyanoperylenediimide (PDI-$8CN_2$) and PDI-FCN_2 films deposited at $T_d = 130$ °C. The SiO_2 surface treatments have modest effects on PDI-$8CN_2$ OFET mobilities, but modulate the mobility and morphology of PDI-FCN_2 films substantially. Most importantly, the surface treatments result in substantially increased V_{th} and decreased I_{off} values for the dicyanoperylenediimide films relative to those grown on SiO_2, resulting in $V_{th} > 0.0$ V and I_{on}/I_{off} ratios as high as 10^8. Enhancements in current modulation for these high-mobility, air-stable, and solution-processable n-type semiconductors, should prove useful in noise-margin enhancement and further improvements in organic electronics.

1. Introduction

The rapidly developing organic electronics field has yielded a wide variety of small molecule/polymeric semiconductors for organic field-effect transistors (OFETs) with the ultimate goal being inexpensive, low power consumption organic complementary circuits (organic-CMOS), having sufficient operating speeds for applications such as displays and RF-ID tags.[1] Until recently, progress toward organic-CMOS circuitry was largely hindered by the lack of organic semiconducting materials which enable high-mobility, low threshold voltage (V_{th}), and environmentally stable n-channel OFETs having sufficient current on-off ratios (I_{on}/I_{off}) for circuit design.[2] However, new strategies in materials design for n-channel OFETs have led to significant electrical parameter enhancement and to improved circuit performance. To this end, the recent fabrication of environmentally-stable organic complementary circuits achieving record operating speeds,[3] ultra-low power consumption,[4] and the first entirely solution-processed active regions[5a] have demonstrated the marked improvements in n-channel device materials. However, the noise margins of these circuits could in principle be enhanced further by improved current modulation in the n-channel transistors, now typically fabricated with $CuF_{16}Pc$ and PDI-$8CN_2$ films (Fig. 1). These air-stable materials have lower current modulation characteristics than many air-sensitive materials used to fabricate n-channel thin film transistors (TFTs), as quantified by the current on-off ratios.[3a,b,5]

Dicyanated arylene diimide semiconductors based on perylene (PDIs) and naphthalene (NDIs) cores receive significant attention because of the unique combination of high electron mobility, environmental electron stability, solution-processability, and compatibility with organic-CMOS design.[3a,b,5a,c–f] However, these materials typically exhibit modest I_{on}/I_{off} ratios ($\sim 10^2$–10^4), primarily due to the high I_{off}. In a recent study, we reported the influence of molecular geometry and LUMO energetics on electron mobility and air-derived charge traps in optimized arylene diimide films grown on bare SiO_2 substrates.[5f] Furthermore, we demonstrated a correlation between the dicyanated arylene semiconductor electron affinity and high I_{off} values, suggesting, that

[*] Prof. M. R. Wasielewski, Prof. T. J. Marks, Dr. B. A. Jones, Dr. A. Facchetti
Department of Chemistry, International Institute for Nanotechnology
Northwestern University
2145 Sheridan Road, Evanston, IL, 60208-3113 (USA)
E-mail: m-wasielewski@northwestern.edu
t-marks@northwestern.edu
Prof. M. R. Wasielewski, Prof. T. J. Marks, Dr. B. A. Jones, Dr. A. Facchetti
Argonne-Northwestern Solar Energy Research Center (ANSER)
Northwestern University
2145 Sheridan Road, Evanston, IL, 60208-3113 (USA)

[**] The authors thank DARPA (HR0011-05-1-0012), AFOSR (STTR FA9550-05-0167), ONR (N00014-05-1-0021 and N00014-05-1-0766), and Polyera Corp. for support of this research, and the NSF-MRSEC program through the Northwestern Materials Research Center (Grant DMR-0520513) for access to characterization facilities.

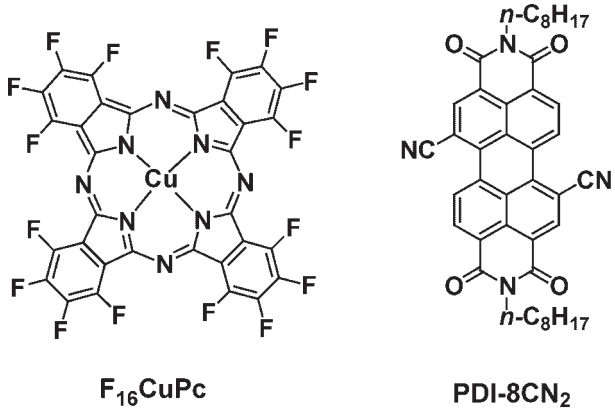

Figure 1. Molecular structures of the most commonly used semiconducting materials for air stable n-channel transistors in organic-CMOS circuitry, $CuF_{16}Pc$ and $PDI\text{-}8CN_2$.

the large carrier concentrations in the ''off'' state of OFETs fabricated with these materials are related to unintentional doping of the energetically low-lying LUMOs.[5f]

Herein, we report on the effects of bulk thin film properties on PDI and NDI charge transport and current modulation. We investigate substrate temperature (T_d) variation during vapor-phase semiconductor film growth for a series of n-channel arylene diimide-based OFETs and the effects of SiO_2 dielectric surface modification on the films of soluble derivatives that yield air-stable transistors. Correlation of semiconductor thin film morphology/microstructure as assessed by AFM and XRD with OFET response parameters is used to understand the influence of film growth conditions on the resulting thin films. In addition, optical absorption spectroscopy is used to qualitatively characterize the semiconductor/chromophore thin film characteristics. Finally, the role of semiconductor deposition temperature (T_d) and dielectric surface modification on OFET performance parameters is discussed, and the first high mobility, air-stable, n-channel, dicyanoarylene diimide OFETs having large I_{on}/I_{off} ratios are demonstrated.

2. Results

2.1. Substrate Temperature (T_d) Effects on Arylene Diimide Semiconductor Film Growth

The synthesis of PDI-8, $PDI\text{-}8Br_2$, $PDI\text{-}8Cl_4$, NDI-8CN, $PDI\text{-}8CN_2$, $PDI\text{-}FCN_2$, and $NDI\text{-}8CN_2$ semiconductors (Fig. 2) was reported previously.[5d,f] Top-contact bottom-gate OFET substrates were fabricated by solvent cleaning, followed by O_2 plasma cleaning. Semiconductor thin films were deposited at $T_d = 70$, 90, 110, and 130 °C by physical vapor deposition and were characterized by X-ray diffraction, tapping-mode atomic force microscopy (AFM), and OFET measurements.

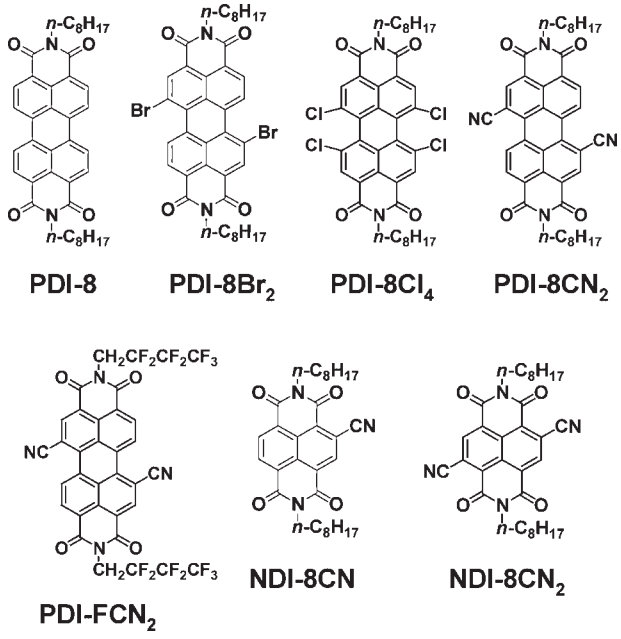

Figure 2. Arylene diimide molecular semiconductors used in this study. The $PDI\text{-}8Br_2$, $PDI\text{-}8CN_2$, and $PDI\text{-}FCN_2$ samples also contain the 1,6 substitutional isomer in addition to the depicted 1,7 isomer.

2.1.1. XRD and Microstructure of Arylene Diimide Thin Films on SiO_2 Deposited at Various T_d

Thin film X-ray diffraction (XRD) is crucial for evaluating the out-of-plane ordering of layered polycrystalline vapor-deposited small-molecule organic thin films, which often correlates with electron mobility. Positions of 2Θ reflections give lattice plane *d*-spacings, while the presence of multiple reflections from the same Bragg family indicates long-range order. Laue oscillations around the first-order diffraction peak indicate extremely uniform layer spacing, while narrowness of the rocking curve full-width-at-half-maximum (FWHM) indicates the quality of the crystallite texturing. An extensive analysis comparing XRD data for optimal films of these semiconductors has been recently presented;[5d,f] therefore, we focus here on the subtle XRD changes with T_d for the individual materials. The average *d*-spacings and the corresponding molecular tilt angles relative to the substrate normal estimated from the *d*-spacings and calculated molecular lengths[5f] are given in Table 1. Assignments of Bragg reflections are based on previous assignments.[5f,6]

In general, the Θ/2Θ scans for all the semiconductor thin films, with the exception of $PDI\text{-}8Cl_4$ and $NDI\text{-}8CN_2$, are similar over the T_d range (70–130 °C) used in this study (Figs. S1–S7). The films exhibit reflections at the same values of 2Θ and the rocking curve FWHM typically remains invariant with T_d; however, the relative intensity of the higher order reflections relative to the first-order reflection often increases with increasing T_d (Fig. 3a and b). The consistency in reflection positions indicates the presence of one polymorph across the T_d range. The increase in relative intensity of the higher order

ADVANCED FUNCTIONAL MATERIALS

Table 1. Thin film X-ray diffraction data for each semiconductor averaged over all T_d, indicating d-spacing, estimated tilt angle from the substrate plane normal, and rocking curve FWHM for the first-order reflection. If the standard deviation for a parameter is less than 5 %, it is not given.

Semiconductor	*d*-spacing [Å]	Tilt angle [°]	ω_{FWHM} [°]
PDI-8	20.5 (0.2)	43	0.03
PDI-8Br_2	22.5 (0.3)	48	0.06
PDI-8Cl_4 (LT)	18.0 (0.1)	36	0.03
PDI-8Cl_4 (HT)	19.6 (0.1)	40	0.03
NDI-8CN	18.2 (0.2)	44	0.03
PDI-8CN_2	19.8 (0.1)	41	0.03
NDI-8CN_2 (LT)	18.2	44	0.03
NDI-8CN_2 (HT)	20.2	50	0.03
PDI-FCN_2	19.5	59	0.05

peaks going from 70 to 130 °C indicates improvements in long range order. For films that exhibit Laue oscillations around the 001 reflection, the oscillations are present at all T_d and correspond to 50 nm. Uniquely, rocking curves of the 001 reflection of PDI-8Br_2 films become more ill-defined and less-intense with increasing T_d, indicating decreased film texturing for this semiconductor at higher T_d (Fig. S2).

In contrast to the other *n*-octyl materials of this study, PDI-8Cl_4 and NDI-8CN_2 films exhibit multiple families of reflections, the relative intensities of which depend on T_d and that correlate with different polymorphs or growth orientations of the semiconductor (Fig. 3c and d). The polymorph with the larger *d*-spacing that becomes more prominent at higher T_ds (HT) is labeled 001′ and the smaller *d*-spacing polymorph more prevalent at low T_d (LT) is labeled 001. For PDI-8Cl_4 films, the LT polymorph is the most prevalent at $T_d = 70$–90 °C (Fig. 3). However, for growth at $T_d = 110$ °C, XRD of the PDI-8Cl_4 films reveals a HT polymorph 001′ reflection that is dwarfed by the LT 001 reflection, as well as a HT 002′ reflection that is well-resolved and of comparable intensity to the LT 002 peak. At $T_d = 130$ °C, the HT polymorph is more prominent than at lower T_d in the XRD, with 001′ to 004′ reflections visible. The LT reflections are more intense than the HT reflections with the exception of 002 versus 002′. Films of NDI-8CN_2 also exhibit LT and HT polymorphs/orientations, which become apparent in the XRD scans at $T_d \geq 90$ °C; however, the NDI-8CN_2 HT polymorph remains much less intense than the LT polymorph over the entire T_d range investigated.

2.1.2. AFM and Morphology of Arylene Diimide Thin Films Deposited on SiO_2 at Various T_d

The surface morphology of an organic semiconductor thin film is often used to evaluate grain size and structure; however, the relevance of these data to OFET performance assumes that the surface morphology is also characteristic of the thin film interface with the substrate, which is the active region for charge transport. Typically, thin film continuity and minimization of grain boundaries are thought to enhance charge transport efficiency. The tapping mode AFM images reveal similar polycrystalline film morphologies for all of the present PDI and NDI derivatives except PDI-8Br_2 (Fig. 4 and Figs. S8–S14). For films of the non-halogenated semiconductors, crystallite size tends to increase with increasing T_d. For the two naphthalene diimide-based materials, the increasing grain size results in pronounced microcracking at $T_d \geq 110$ °C, leading to film discontinuities at higher T_d. Additionally, films of the non-halogenated semiconductors tend to exhibit protruding surface crystallites at lower T_d, which become less prevalent as T_d increases. Interestingly, films of NDI-8CN and NDI-8CN_2 do not evidence protruding surface crystallites at any T_d utilized in this study (Fig. 4). The surface morphology of PDI-FCN_2 films reveals a dramatic decrease in large plate-like surface protrusions as T_d increases to 110 °C, but the presence of small round surface crystallites appears at ~130 °C. Interestingly, similar surface crystallites have been observed in other vapor-deposited small molecule films, which were attributed to a different film orientation.[7] Since we do not observe new reflections in the XRD that correlate with the surface protrusions, they may be amorphous regions.

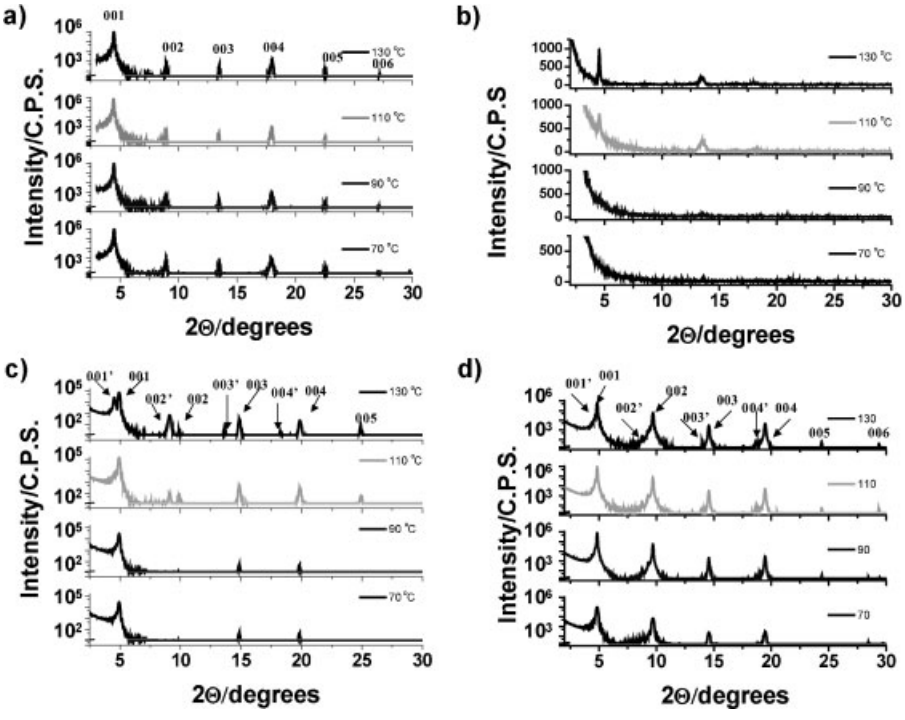

Figure 3. Representative Θ/2Θ X-ray diffraction scans of a) PDI-8CN_2, b) PDI-FCN_2, c) PDI-8Cl_4, and d) NDI-8CN_2 films deposited at the indicated T_d values.

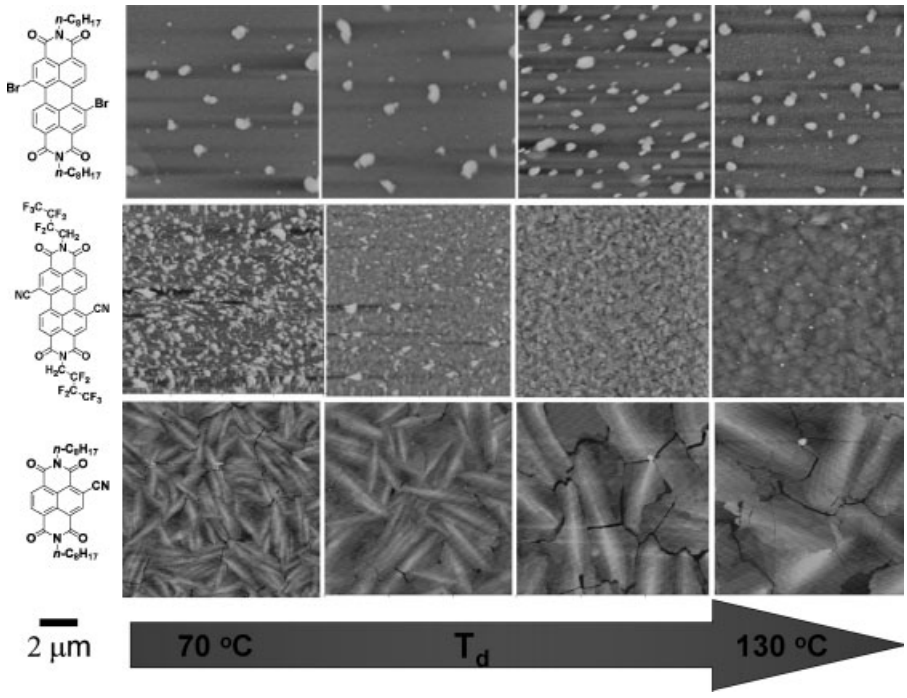

Figure 4. Representative AFM images of (top) PDI-8Br_2 films, (middle) PDI-FCN_2, and (bottom) NDI-8CN films deposited at the indicated T_d values.

The films of the two halogenated semiconductors exhibit significantly different film morphologies versus the previously discussed materials. The film morphology in the case of PDI-8Br_2 does not exhibit the sharp grain boundaries evident in films of the other semiconductors investigated in this study (Fig. 4). Furthermore, surface protrusions are obvious at all T_d values, which are large in dimensions and sparse at $T_d = 70\,^{\circ}C$, but become smaller and denser as T_d increases.

In the case of PDI-8Cl_4, the increasing grain size with T_d also results in microcracking at $T_d \geq 110\,^{\circ}C$, and by $T_d = 130\,^{\circ}C$, there are interestingly two distinct film morphologies detectable. One film topology is related to the plate-like morphology observed at lower T_d (LT); however, the grain boundaries and plates become more well-defined versus those grown at lower T_ds. The new film morphology (HT) exhibits less prevalent grain boundaries in the film structure, which is comprised of elongated grains.

2.1.3. OFET Measurements in Vacuum for Thin Films Deposited on SiO_2 at Various T_d Values

With the exception of PDI-8Br_2 and PDI-FCN_2, OFET electron mobilities are invariably lowest at $T_d = 70\,^{\circ}C$ and show little change between $T_d = 90$ and $130\,^{\circ}C$ (Fig. 5). PDI-8Br_2 devices exhibit a maximum average mobility of $3 \times 10^{-5}\,cm^2\,V^{-1}\,s^{-1}$ at $T_d = 70\,^{\circ}C$, with the mobility then decreasing with further increases in T_d. Compared to the *N*,*N*′-*n*-octyl semiconductors, the electron mobility of PDI-FCN_2 devices is very sensitive to T_d. The mobility increases from $10^{-7}\,cm^2\,V^{-1}\,s^{-1}$ for semiconductor films deposited at $T_d = 70\,^{\circ}C$ to $0.31\,cm^2\,V^{-1}\,s^{-1}$ for films deposited at $T_d = 130\,^{\circ}C$.

Threshold voltages (V_{th}) remain relatively constant over the T_d range used in this study, again with the exception of PDI-8Br_2 and PDI-FCN_2 (Table S1). The value of V_{th} for each individual semiconductor generally decreases with increasing electron affinity, as discussed in previous work.[5f] The standard deviation in V_{th} for PDI-8Br_2 is very large, probably reflecting the unusual film morphology/microstructure as discussed earlier. The large variation of V_{th} over the T_d range for PDI-FCN_2 TFTs is most likely due to improvements in film morphology/microstructure at higher T_ds that minimize trap densities, thus shifting V_{th}. While I_{on} and I_{off} generally increase with increasing T_d, the I_{on}/I_{off} ratio typically remains unchanged over the T_d range surveyed in this study. I_{on} is taken at $V_g = +100\,V$ for each device, while I_{off} is the lowest current observed during the V_g sweep from $-100\,V$ to $+100\,V$. The maximum I_{on}/I_{off} ratios observed for OFETs of the indicated semiconductors are 10^7 for PDI-8, 10^3 for PDI-8Br_2, 10^5 for PDI-8Cl_4, 10^5 for NDI-8CN, 10^4 for PDI-8CN_2, 10^3 for NDI-8CN_2, and 10^3 for PDI-FCN_2 (Table S1)

2.2. Substrate Treatment Effects on Dicyanoperylenediimide Semiconductor Film Growth

Since PDI-8CN_2 and PDI-FCN_2 have demonstrated great promise as high-mobility, air-stable, solution-processable semiconductors for organic-CMOS,[3a,b,5a,c,e] these materials were selected for further investigations on the different gate insulator substrates. Some OFET substrates were utilized for

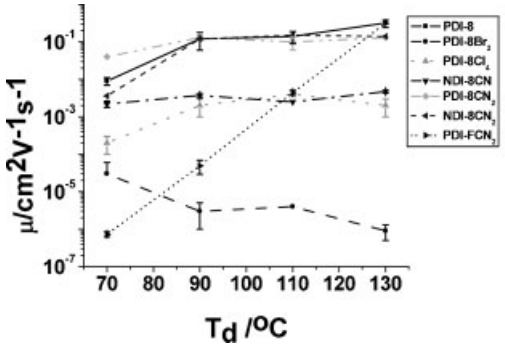

Figure 5. OFET electron mobility as a function of T_d for the seven arylene diimide semiconductor films of this study grown on bare SiO_2.

ADVANCED FUNCTIONAL MATERIALS

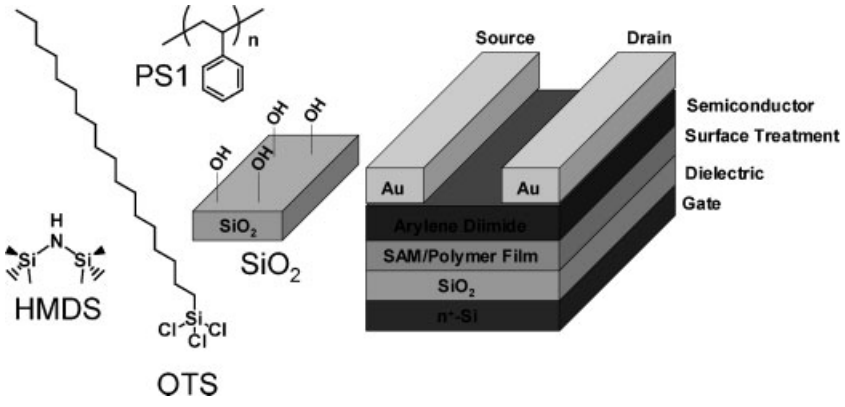

Figure 6. (left) Gate dielectric surface treatments explored in this study, and (right) device structure of a gate dielectric functionalized top-contact bottom-gate OFET used in this study.

semiconductor thin film deposition after cleaning to provide a clean bare-SiO_2 substrate (designated SiO_2). Subsequently, a surface modification as described below was applied to the SiO_2 dielectric (Fig. 6).[8] For substrates modified with self-assembled monolayers (SAMs), multiple deposition techniques were investigated. Hexamethyldisilazane-modified substrates were fabricated by exposing SiO_2 substrates to hexamethyldisilazane vapor for ~20 d in a nitrogen atmosphere to yield a trimethylsilyl-coated interface (aqueous contact angle ~97°) between the dielectric and semiconductor thin film. Substrates treated with HMDS for shorter times (3 d) or immersed in neat HMDS for 24 hours at room temperature give aqueous contact angles ~90°; however, the OFETs fabricated with the substrates treated with HMDS for 24 h and 3 d exhibit V_{th} and I_{off} parameters similar to those on bare SiO_2 substrates (Fig. S16). This suggests incomplete surface coverage of the SiO_2 substrates for the shorter HMDS treatment duration, consistent with previous reports.[9] Therefore, any further references to HMDS-treated SiO_2 substrates (designated HMDS) refer to those treated for ~20 d.

Octadecyltrichlorosilane-modified substrates (designated OTS) were fabricated by immersion of the SiO_2 substrates in 3.0 mM dry dichloromethane solutions of the silane reagent under nitrogen for 24 hours to yield a *n*-octadecyl-coated interface.[8a,10] Additionally, polystyrene-coated substrates were fabricated by spin-casting (5000 rpm) a 5.0 mg mL^{-1} toluene solution of polystyrene onto the SiO_2 substrates (designated PS1).[11] All substrates were characterized by advancing aqueous contact angle measurements, which indicate decreasing hydrophilicity in the order: SiO_2 ($\Theta < 5°$), PS1 (91°), HMDS (97°), and OTS (104°). Additionally, surface roughness was evaluated by tapping mode AFM, revealing RMS roughnesses of 0.87 nm for SiO_2, 1.2 nm for HMDS, 0.92 nm for PS1, and 1.9 nm for OTS (Fig. S15).

2.2.1. XRD of Dicyano PDIs as a Function of Substrate Treatment

Films of PDI-8CN_2 ($T_d = 130$ °C) reveal essentially the same $\Theta/2\Theta$ X-ray diffraction characteristics on all the substrates investigated in this study (Fig. 7). These characteristics are discussed in detail above. The rocking curves of the 001 reflections for both PDI-8CN_2 films and PDI-FCN_2 on SiO_2-, HMDS- and OTS-substrates exhibit intense narrow peaks characteristic of highly textured films, but films on PS1 exhibit significant broadening and more noisy rocking curves, which indicates significantly less texturing (Figs. S17 and S18).

2.2.2. AFM Images of Dicyano PDI Films on Various Substrates

The film morphology of PDI-8CN_2 and PDI-FCN_2 films grown on different sub-

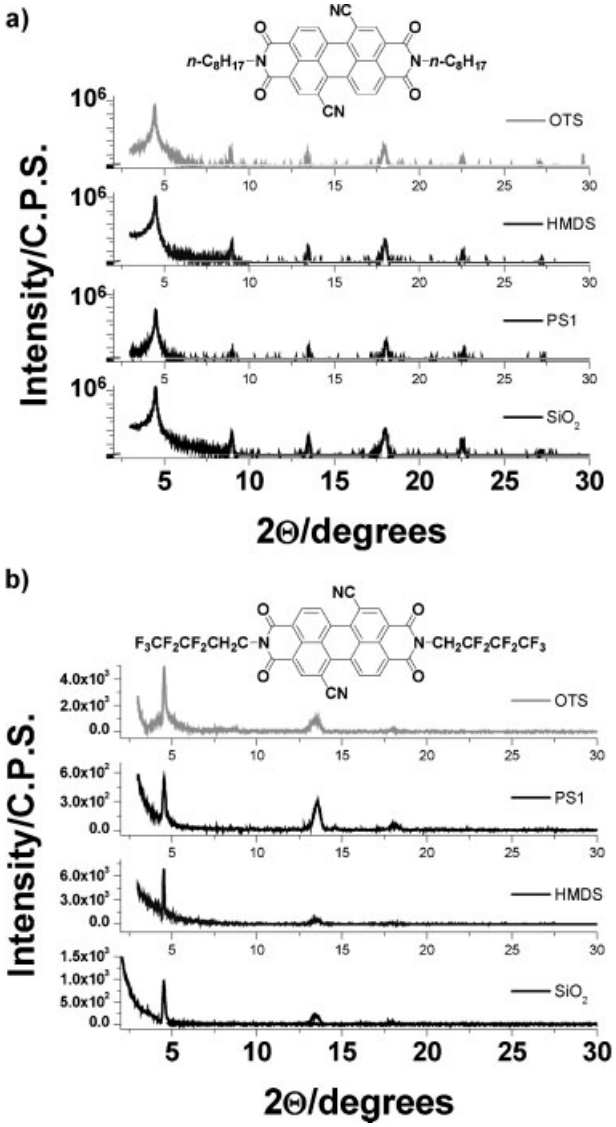

Figure 7. $\Theta/2\Theta$ X-ray diffraction scans of: a) PDI-8CN_2 films and b) PDI-FCN_2 films deposited on the indicated substrates ($T_d = 130$ °C) with the gate dielectric surface treatments indicated.

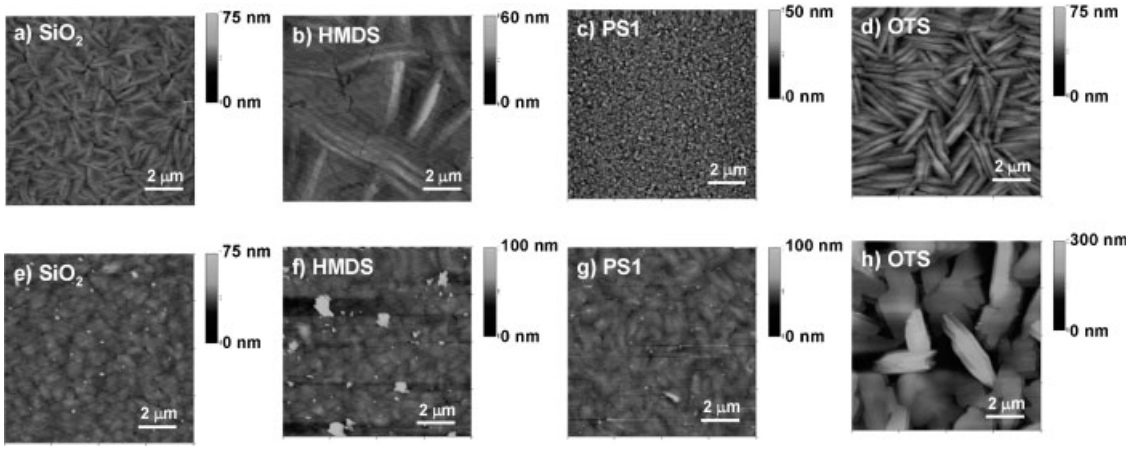

Figure 8. AFM images of PDI-8CN_2 films on a) bare SiO_2, b) HMDS-, c) PS1-, and d) OTS-treated gate dielectrics and PDI-FCN_2 films deposited on a) bare SiO_2, b) HMDS-, c) PS1, and OTS-treated gate dielectric substrates.

strates as characterized by tapping-mode AFM varies greatly (Fig. 8). In the case of PDI-8CN_2, the film morphologies on bare SiO_2, HMDS-, and OTS-treated SiO_2 substrates exhibit a ribbon-like grain structure. The grains on HMDS-treated SiO_2 are significantly more elongated versus those on SiO_2, and clear terraces can be observed. On bare SiO_2 and HMDS-treated SiO_2, large plate-like areas with grain boundaries can be observed as well. PDI-8CN_2 films grown on OTS-treated substrates also exhibit elongated crystallites; however, terraces and plate-like regions are not observed. In contrast, the PDI-8CN_2 films grown on PS1 surfaces exhibit smaller grains. The PDI-FCN_2 film morphology is relatively constant for films grown on SiO_2, PS1, and HMDS. The films on SiO_2 and HMDS produce similar granular structures; however, films on SiO_2 have small round structures protruding from the surface, and on HMDS the protruding features become larger and more irregularly shaped. PDI-FCN_2 films grown on PS1, SiO_2, and HMDS substrates exhibit similar grain structures and small, round surface features.

2.2.3. Optical Spectra of Dicyano PDI Films on Various Substrates

Optical spectroscopy can be utilized as an indicator of the relative proximity/orientation of the adjacent chromophore transition dipoles, which typically lie along the molecular long-axes.[2] These effects have been extensively studied in perylene diimide-based materials to characterize crystallochromic behavior and the structures of solution-phase molecular assemblies.[12] The spectra of perylene diimide chromophores aligned face-to-face with the molecular long axes nearly in registry (termed an H-aggregate) exhibit characteristic absorption spectra in which the oscillator strength of the higher energy transitions (the absorption band ~485 nm in the case of the present dicyanated PDIs) are enhanced relative to the lowest energy band.[12a,o,q,13] If the transition dipoles of two adjacent perylene chromophores are translated toward a ''head-to-tail'' orientation (termed a J-aggregate), the absorption spectrum redshifts significantly.[12a,13] Note that these are qualitative descriptions of H- and J-aggregation, and in thin films the interpretation becomes less straightforward.[2a,b,13,14] In the case of perylene diimide thin films exhibiting very high-quality layering, indications of relative transition dipole orientations could prove informative in understanding in-plane packing arrangements, which cannot be straightforwardly evaluated by conventional thin film diffraction techniques. However, optical absorption spectroscopy probes the bulk film, which is not necessarily representative of the semiconductor active region. Given that the Laue oscillations in the XRD correlate almost exactly with the thin film thickness for the non-brominated *N*,*N*′-*n*-octyl materials, the assumption that the bulk orientation is representative of the interface seems reasonable in these cases.

Films of PDI-8CN_2 and PDI-FCN_2 were grown on glass substrates pretreated in the same manner as that described above. For films of PDI-8CN_2, the optical spectrum is relatively insensitive to substrate treatment (Fig. 9). Relative to the solution phase spectrum in dichloromethane where the absorption maximum is at 522 nm, the thin film spectrum absorption maximum is red-shifted to ~550 nm, characteristic of J-type aggregation. For films of PDI-FCN_2, the solution phase spectrum has an absorption maximum at 523 nm (Fig. 9b), while films of PDI-FCN_2 on SiO_2, HMDS, and PS1 exhibit absorption spectra characteristic of H-like aggregation. The films of PDI-FCN_2 on OTS exhibit a substantially redshifted and broadened absorption spectrum, which could be attributed to either J-like aggregation or exciton delocalization. Since the position and the intensities of the reflection in the XRD of films on OTS versus the other substrates remains similar, the redshifted absorption spectrum of films grown on OTS can likely be attributed to delocalized excitons in vapor-deposited perylene diimide thin films.[15] This characteristic absorption spectrum has been shown to accompany substantially increased crystal grain size,[15] which is consistent with the present AFM data for the PDI-FCN_2 films grown on OTS-treated substrates versus the other surface treatments.

ADVANCED FUNCTIONAL MATERIALS

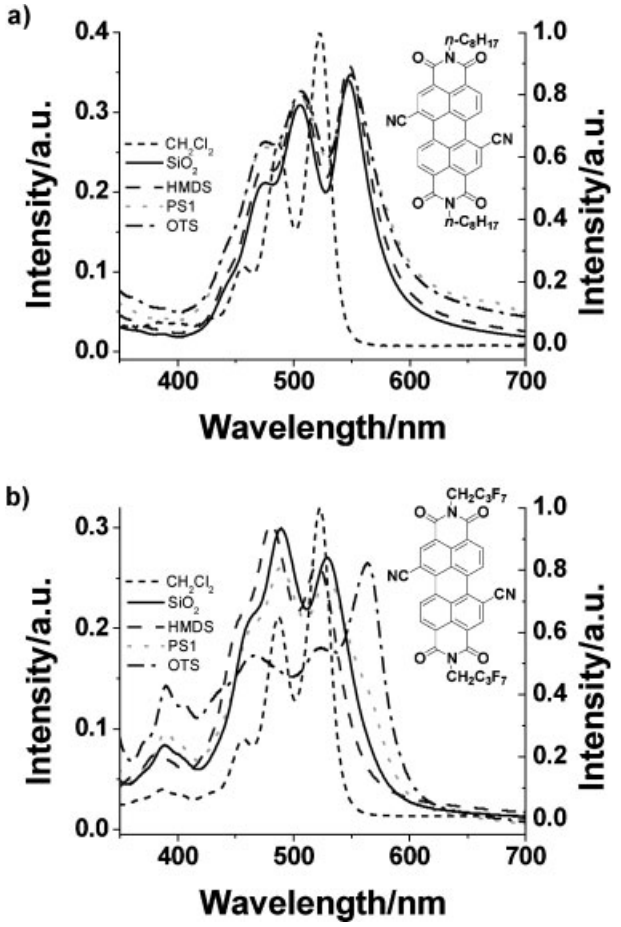

Figure 9. Optical absorption spectra of a) PDI-8CN_2 films deposited on glass substrates having varying treatments and b) PDI-FCN_2 films deposited on glass substrates having varying surface treatments. Spectra of PDI-8CN_2 and PDI-FCN_2 in dichloromethane solution are presented for comparison.

2.2.4. OFET Measurements of Dicyano PDIs on Various Substrates

Dielectric surface treatment variation results in appreciable tuning of the OFET electron mobility, V_{th}, and I_{on}/I_{off} (Table 2). The PDI-8CN_2 transistor electron mobilities show minor variation with the exception of films on PS1 substrates, which display substantially lower values. PDI-FCN_2-based transistors on treated and SiO_2 substrates yield devices with the highest average electron mobilities on HMDS, and the values on SiO_2 are only slightly lower. The PDI-FCN_2 transistor mobilities on PS1 and OTS substrates yield similar but lower values than on HMDS and SiO_2.

The V_{th} values of both the PDI-8CN_2 and PDI-FCN_2 devices evidence dramatic variations as a function of gate dielectric surface treatment (Table 2). For both PDI-FCN_2- and PDI-8CN_2-based devices, the average V_{th} is significantly more positive on the treated substrates compared with the devices fabricated on bare SiO_2 substrates.

The I_{on}/I_{off} ratios of both PDI-8CN_2 and PDI-FCN_2 devices evidence large variations, depending on the surface treatment,

Table 2. Organic Field-Effect Transistor Characteristics for the indicated vapor deposited semiconductor thin film ($T_d = 130\,^\circ C$) measured in vacuum. Saturation regime electron mobilities (μ) are given in $cm^2\ V^{-1}\ s^{-1}$, threshold voltages (V_{th}) are given in volts [V], and current on-off ratios (I_{on}/I_{off}) are given for $V_g = +200$ V to $V_g = -50$ V.

Treatment	μ	V_{th}	I_{on}/I_{off}
PDI-8CN_2			
SiO_2	0.12 (0.03)	−9 ((4)	10^3
PS1	0.01 (0.003)	15 (5)	10^7
OTS	0.06 (0.01)	27 (1)	10^8
HMDS	0.10 (0.01)	11 (3)	10^7
PDI-FCN_2			
SiO_2	0.31 (0.07)	−21 (4)	10^3
PS1	0.13 (0.03)	18 (7)	10^6
OTS	0.15 (0.05)	−3 (10)	10^7
HMDS	0.53 (0.06)	15 (3)	10^6

and the trends parallel those for V_{th} (Table 2). The differences in I_{on}/I_{off} are primarily due to changes in I_{off}, given that changes in I_{on} vary less than one order of magnitude, while J_{off} varies as much as $\sim 2 \times 10^6\ A\,cm^{-2}$ ($10^3\times$) in PDI-FCN_2 devices and by $\sim 2 \times 10^8\ A\,cm^{-2}$ ($10^5\times$) in PDI-8CN_2 devices (Fig. 10).

3. Discussion

3.1. Correlations between T_d, OFET Response, and Thin Film Microstructure/Morphology

In the context of the present PDI- and NDI-based OFETs, varying the film growth temperature (T_d) between 70 and 130 °C results in only minor changes in OFET electrical parameters for the *N*,*N*′-*n*-octyl substituted arylene diimide derivatives having high microstructural order. Often, electron mobility and I_{on}/I_{off} are about one order of magnitude lower for $T_d = 70\,^\circ C$ than for $T_d > 70\,^\circ C$, which affords optimal performance (Fig. 5 and Table S1). Since the *d*-spacings and rocking curves for these materials are nearly indistinguishable at all T_d, the less optimal device response parameters typically seen in $T_d = 70\,^\circ C$ films are reasonably attributed to thin film microstructure and long-range order.

Inspection of the Θ/2Θ XRD data at $T_d = 70\,^\circ C$ for the *N*,*N*′-*n*-octyl materials shows that the reflections higher in order than 001 are significantly weaker than for the higher T_d films (Figs. S1–S7). The presence of intense high-order reflections is associated with long range order in these layered polycrystalline thin films; therefore, the device performance enhancements frequently observed for growth between $T_d = 70$ and 90 °C can be at least partly associated with increases in long range order at the higher T_ds. In the case of NDI-8CN films, which yield OFETs with nearly identical parameters at all T_ds investigated, higher order diffraction features are present at all T_d. The PDI-8Cl_4-based OFETs exhibit small variations in electrical parameters from $T_d = 90$ to 130 °C which are statistically significant, and which can most likely be attributed to the simultaneous presence of HT and LT polymorphs over this growth temperature range.

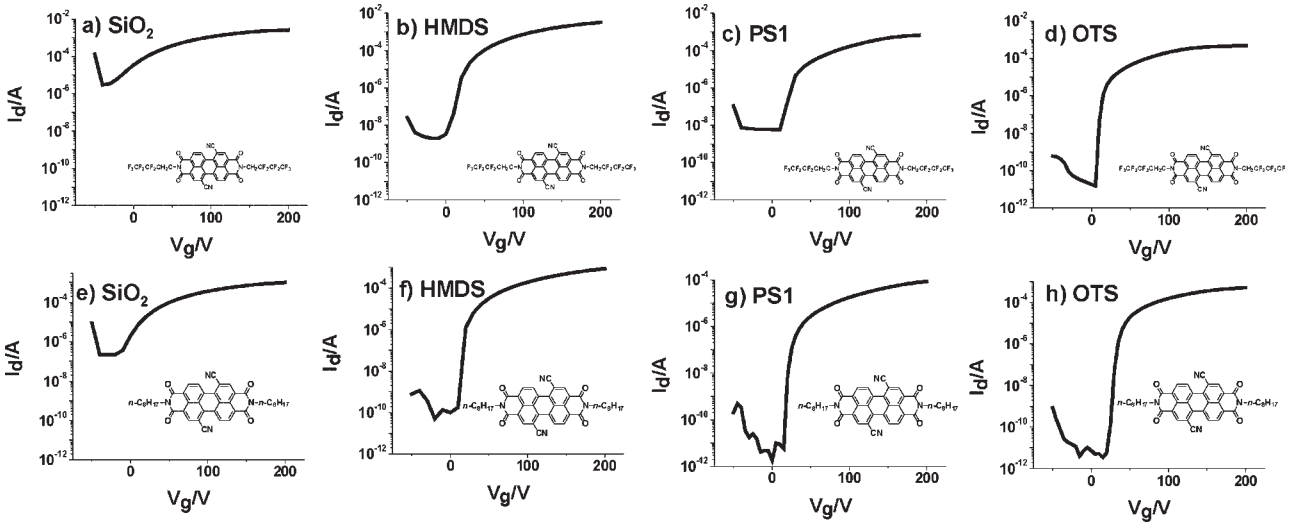

Figure 10. Transfer plots showing I_d as a function of V_g for PDI-8CN$_2$ films deposited at $T_d = 130\,^{\circ}C$ on: a) SiO_2 substrates, b) HMDS substrates, c) PS1 substrates, and d) OTS substrates, as well as PDI-FCN$_2$ films deposited at $T_d = 130\,^{\circ}C$ on: e) SiO_2 substrates, f) HMDS substrates, g) PS1 substrates, and h) OTS substrates.

In addition to the XRD, the AFM surface morphology characterization suggests that the surface features present in PDI-8, PDI-8CN$_2$, and NDI-8CN$_2$ films deposited at $T_d = 70\,^{\circ}C$ are partially responsible for the less than optimal OFET response (Figs. S8, S12, and S13). NDI-8CN films do not exhibit surface protrusions at any T_d used in this study, and the OFET parameters exhibit minimal variation outside the standard deviations (Fig. 5). In contrast, the PDI-8Cl$_4$ film surface morphology reveals increases in grain size which parallel increases in OFET electron mobility until $T_d = 110\,^{\circ}C$. The slight decrease in electron mobility for PDI-8Cl$_4$ films deposited at $T_d = 130\,^{\circ}C$ may be due to the simultaneous presence of the HT and LT polymorphs, observable in both the AFM and XRD images (Fig. S10). Additionally, AFM studies suggest that the crystallite grain size is typically much smaller at $T_d = 70\,^{\circ}C$, which, all things being equal, should result in more film grain boundaries, hence more trapping sites.[16] At $T_d > 70\,^{\circ}C$, the grain size becomes larger, which should work to minimize trap density contributions from grain boundaries.[16]

The cases of PDI-FCN$_2$ and PDI-8Br$_2$ films are unique because they display large excursions in OFET electron mobility and I_{on}/I_{off} parameters over the T_d range utilized in this study. Devices fabricated with PDI-FCN$_2$ thin films exhibit very large gains in electron mobility as T_d is increased from 70 to 130 °C (Fig. 5). Analysis of film morphology by tapping-mode AFM reveals a large density of protruding features from the film surface at $T_d = 70\,^{\circ}C$, similar to the case of many of the other low mobility films. The density of the surface features decreases as T_d is increased to 110 °C, which is accompanied by significant increases in electron mobility (Fig. S14). At $T_d = 110\,^{\circ}C$, cracking/grain boundaries are noticeable in the film morphology, however the film becomes more continuous at $T_d = 130\,^{\circ}C$, which likely reduces trap density and is observed to result in improved electron mobility. Also at $T_d = 130\,^{\circ}C$, surface protrusions begin to appear on the PDI-FCN$_2$ thin film again, suggesting that mobility could be optimized further, given the pronounced electron mobility depression that typically accompanies these features in the arylene diimide thin films studied here.

In contrast to the above results, PDI-8Br$_2$ devices exhibit optimal mobility and I_{on}/I_{off} at $T_d = 70\,^{\circ}C$, which then erode with increasing T_d (Fig. 5). XRD scans of the PDI-8Br$_2$ films yield similar $\Theta/2\Theta$ XRD data at all T_d values. However, the 001 reflection for the $T_d = 130\,^{\circ}C$ film is weak, suggesting less microstructural order. The weak and ill-defined rocking curves for PDI-8Br$_2$ films suggest greater variation in crystallite orientation compared to the other *N,N′-n*-octyl materials, and the intensity of these curves tends to decrease with increasing T_d (Fig. S2). Together, these data suggest that the out-of-plane microstructural order decreases with increasing T_d in PDI-8Br$_2$ film growth, partially explaining the electrical parameter decline with increasing T_d. Additionally, the AFM data show that surface protrusions are present in PDI-8Br$_2$ films at all T_ds investigated in this study, and the density of these features increases with T_d. The presence of large numbers of presumably amorphous surface features in the AFM consistently parallels lower electron mobilities in the PDI-8, PDI-8Br$_2$, PDI-8CN$_2$, and NDI-8CN$_2$ films of this study, suggesting that such features impede rapid charge diffusion through these thin films. The large V_{th} variation in PDI-8Br$_2$ films reflects the poor semiconductor properties, which are most likely due to the unique and unfavorable film microstructure/morphology. The cause of the variations in thin film properties due to arylene diimide functionalization may be due to the differences in crystal packing often associated with functionalization, as seen in other work.[5f,12b]

V_{th} variation as a function of T_d during arylene diimide film growth on SiO_2 is small or negligible for all the semiconductors of this study, with the exception of PDI-8Br$_2$ and PDI-FCN$_2$. As discussed in previous work,[5f] the V_{th} values of all of these

ADVANCED FUNCTIONAL MATERIALS

materials closely track the trends in reduction potential/LUMO energetics, provided the films have similar microstructures/morphologies and are grown on identical substrates. The significant V_{th} variation observed in PDI-8Br$_2$ transistors is probably due to the poor film quality as indicated by the wide rocking curves, lack of higher order diffraction peaks, and the presence of large densities of film surface protrusions, as discussed earlier. The large trap density associated with poor film quality that leads to low electron mobilities will also cause substantial shifts in V_{th}; thus, for the particularly poor OFETs fabricated with PDI-8Br$_2$ thin films grown between 90–130 °C, V_{th} becomes erratic. Similarly, PDI-FCN$_2$ films deposited at $T_d < 110$ °C exhibit low electron mobilities and poor film texturing, which is likely accompanied by large electron trap densities.

Typically, I_{on}/I_{off} values are the lowest at $T_d = 70$ °C for arylene diimide films grown on SiO_2 but incrementally increase and plateau at $T_d \geq 90$ °C, mirroring the trends in electron mobility (Table S1). This enhanced current modulation is due to increased I_{on} accompanying the increased electron mobility and improvements in film microstructure/morphology at higher T_d. Similarly, the fall in I_{on}/I_{off} with T_d for PDI-8Br$_2$-based devices grown on SiO_2 is due to the decreased I_{on} that accompanies the decreased electron mobility due to the poor film morphology associated with the higher T_ds.

3.2. Dielectric Surface Treatment Effects on Mobility

Surface treatment of the SiO_2 gate dielectric in the present OFETs effects varying degrees of electron mobility modulation, depending on the *N*,*N*′-functionalization. The exact reason for the observed variations in these parameters is difficult to exactly define, given that previous studies revealed that many aspects of these surface treatments, associated with a molecular dipole,[8a,c,10] smoothness,[17] trap density,[11a] thin film growth mechanism,[11a] and surface energy mismatch effects between the thin film and substrate,[11a] can influence OFET response. Since the semiconductor thin films were grown ($T_d = 130$ °C) simultaneously on the four different substrates, the deposition conditions should be identical for each surface. Interestingly, the electron mobilities of PDI-8CN$_2$ devices remain relatively constant for bare SiO_2, HMDS-, and OTS-treated SiO_2 substrates (Table 2). Given that the electron mobilities are identical within experimental uncertainty for the hydrophilic SiO_2 and hydrophobic HMDS-treated surfaces, the substrate surface energy appears to have little effect on the performance quality of PDI-8CN$_2$ OFETs. Additionally, the carrier mobilities of the PDI-8CN$_2$-based devices do not parallel the trends in RMS roughness, which is uniformly ~1 nm. The XRD scans of PDI-8CN$_2$ films on the bare SiO_2, HMDS-, and OTS-treated SiO_2 substrates are very similar; however, the AFM does reveal slight variations in surface morphology (Fig. 8). Thus, the OFET response of PDI-8CN$_2$ films is relatively insensitive to surface hydroxylation or saturated hydrocarbon treated surfaces.

For PDI-8CN$_2$ devices, films grown on PS1 substrates are the only specimens that do not yield OFETs with electron mobility ~0.1 $cm^2 V^{-1} s^{-1}$ (Table S1). Examination of the AFM and XRD data shows that the morphology and microstructure of PDI-8CN$_2$ films grown on PS1 is substantially different from that on the other three substrates. The AFM images reveal much smaller crystallite grains compared to the other substrates, which would suggest more grain boundaries and more electron trapping states (Fig. S12). Additionally, the reflection intensities in the $\Theta/2\Theta$ scan for PDI-8CN$_2$ films on PS1 are weaker than on the other substrates (Fig. 7). Finally, the rocking curve of the PDI-8CN$_2$ *001* reflection on PS1 is too weak to define a FWHM, which suggests greater variations in the order of these films (Fig. S17). Thus, the lower PDI-8CN$_2$ electron mobility on PS1 substrates is ascribed to less ordered films with smaller grains, which in turn should lead to larger electron trap densities.[11b] The optical spectra of PDI-8CN$_2$ films on the different substrates reveals evidence of J-like character. The somewhat lower electron mobility of the J-like PDI-8CN$_2$ thin films relative to the H-like PDI-FCN$_2$ films suggests that differences in relative orientations of some fraction of the dicyano perylene diimide chromophores and thus differences in the π–π overlap in the thin films may be responsible for the higher PDI-FCN$_2$ transistor mobilities.

The electron mobility of PDI-FCN$_2$ FETs is independent of both substrate roughness in the range of this study and surface energetics. The SiO_2 and HMDS-treated substrates yield the highest mobility devices for PDI-FCN$_2$ films; however, the average electron mobility for films grown on HMDS-treated substrates is 0.53 $cm^2 V^{-1} s^{-1}$, while that of SiO_2 substrates is 0.31 $cm^2 V^{-1} s^{-1}$ (Table 2). On OTS and PS1 substrates, the electron mobilities are lower (~0.1 $cm^2 V^{-1} s^{-1}$) and statistically indistinguishable from one another. Interestingly, AFM reveals that the crystalline grain structure of PDI-FCN$_2$ films grown on OTS is substantially different from that on the other three substrates; therefore, a priori, the mobility should be affected (Fig. 8). Furthermore, the optical spectra of the thin films on OTS show evidence of delocalized excitons associated with large grain perylene diimide films, whereas PDI-FCN$_2$ films on the other three substrates show spectra associated with H-type aggregation. Note that calculated absorption spectra for perylene bisimides reveal that minor changes in orientation can lead to substantial shifts in the absorption spectra.[14a,b,18]

3.3. Gate Dielectric Surface Treatment Effects on V_{th} and I_{on}/I_{off}

The effects of surface treatment on V_{th} and I_{on}/I_{off} parallel each other for both PDI-8CN$_2$- and PDI-FCN$_2$-based OFETs (Table 5.5). In the case of SiO_2 substrates for both dicyanated PDIs, V_{th} is negative of 0.0 V, indicating the presence of mobile charge carriers when the transistor is "off" ($V_g = 0.0$ V). The presence of charge carriers under these conditions could be attributed to both unintentional doping by electron-rich

chemical functionalities[5b,c,4a] and/or the presence of local electric fields generating charge carriers in the channel in a similar manner to an applied gate bias.[8a,c,10] Note that the silanol groups on SiO_2 are typically considered electron traps for conjugated organic materials; however, it has been shown that the n-type carriers in conjugated organic materials with $E_{red1} > \sim -0.6$ V versus S.C.E. ($E_{LUMO} \sim -3.8$ eV) are negligibly susceptible to such traps.[11a] Thus, all the semiconductors utilized here with $E_{red1} > -0.5$ V versus S.C.E. should experience minimal trapping by the bare SiO_2 dielectric. When the SiO_2 dielectric is functionalized with HMDS, PS1, or OTS, the V_{th} shifts substantially positive of the value on SiO_2 for the present dicyano perylene diimide-based OFETs. PS1 and HMDS substrates typically yield devices with similar V_{th} values; however, OTS treatment yields the most positive V_{th} of +27 V in PDI-8CN_2 devices and the lowest V_{th} of −3.0 V for the treated SiO_2 substrates in PDI-FCN_2 devices. Therefore, the surface treatments quench dopants and/or alter the aforementioned electric fields at the dielectric/semiconductor interface. A similar positive V_{th} shift has also been observed for C_{60}- and pentacene-based OFETs.[8c]

The enhancement of I_{on}/I_{off} for coated substrates versus bare SiO_2 substrates parallels the trend in V_{th} because the high I_{off} on SiO_2 substrates is the cause of the limited current modulation in these devices. The shift in V_{th} to positive values argues that there must be very few charge carriers in the channel without an applied bias, and the decrease in off current density on coated substrates by $\sim 2 \times 10^6$ A cm^{-2} ($10^3\times$) in PDI-FCN_2 devices and $\sim 2 \times 10^8$ A cm^{-2} ($10^5\times$) in PDI-8CN_2 devices confirms the depletion of charge carriers relative to SiO_2 devices. The shift in V_{th} and increase in I_{on}/I_{off} are significant because the devices can now be operated entirely in enhancement mode to yield air-stable n-channel OFETs with high current modulation. A similar effect, although unnoted, is evident in recently reported $CuF_{16}Pc$ transistor data, suggesting that organic surface treatments can be utilized to address the low current modulation associated with many high electron affinity/air-stable n-type organic semiconductors.[11a,19]

4. Conclusions

Variation of growth temperature (T_d) between 70–130 °C for *N*,*N*′-*n*-octyl arylene diimide semiconductor thin films reveals that OFET electron mobility is the lowest at 70 °C and increases slightly at higher T_d values. The electron mobilities of these materials remain relatively constant between $T_d = 90$ °C and 130 °C. The I_{on}/I_{off} values exhibit a similar trend, and V_{th} remains essentially constant over the T_d range of this study. OFET electron mobility and I_{on}/I_{off} values for PDI-8Br_2 films maximize at $T_d = 70$ °C and decrease with increasing T_d, while V_{th} varies erratically over the T_d range of this study. PDI-FCN_2 films show substantial and systematically varying electron mobility and I_{on}/I_{off} enhancement over the T_d range in this study, while the V_{th} is again erratic. Typically, optimal OFETs fabricated with the arylene diimide semiconductor films of this study exhibit large crystalline grains, minimal surface morphological protrusions, and high-quality order in the XRD.

Examination of SiO_2 substrate surface treatment effects for PDI-8CN_2 and PDI-FCN_2 films deposited at $T_d = 130$ °C reveals that electron mobilities for the two semiconductors are optimal on SiO_2 and HMDS substrates, respectively, signifying little dependence on substrate surface energy. Electron mobilities on OTS substrates are high for PDI-8CN_2 devices, but PDI-FCN_2 adopts a drastically different surface morphology on OTS, leading to depressed carrier mobility. Thin films of both semiconductors on PS1 yield lower than optimal mobilities, which is apparently due to less texturing in the layered thin films. Importantly, treatment of the SiO_2 dielectric with organic surface treatments results in a positive V_{th} shift and significantly decreased I_{off}, which enables fabrication of OFETs without adventitious doping and affords significantly increased current modulation with I_{on}/I_{off} values as high as 10^8. This realization of low I_{off} values in dicyanated arylene diimide semiconductors should prove invaluable in optimizing organic CMOS based on these high-mobility, air-stable, solution-processable, n-type organic semiconductors.

5. Experimental

The arylene diimide syntheses were reported previously.[5c,d,f,20] Hexamethyldisilazane, octadecyltrichlorosilane, and polystyrene ($M_w = 2.8 \times 10^5$) were purchased from Sigma–Aldrich. Highly doped n+-silicon wafers with 300 nm thermally grown SiO_2 dielectric layers were purchased from Montco Silicon Tech. The gate dielectric capacitance is assumed to be 10 nF cm^{-2} for all substrates, in accordance with the literature.[11a] Substrate cleaning and preparation is described above. Thin films (50 nm) of the arylene diimide semiconductors were deposited (0.2 Å s^{-1}) by physical vapor deposition (10^{-6} Torr) at the specified T_d, followed by Au source and drain electrodes ($W/L = 5$ mm/100 μm) which were deposited through a shadow mask to yield top-contact, bottom-gate OFETs. Tapping mode AFM measurements were performed on a Digital Instruments Multimode Nanoscope IIIa with Nanoprobe TESP-70 tips (cantilever length = 125 μm, freq. = 278–338 kHz). X-ray diffraction ($\Theta/2\Theta$ and ω scans) was performed on a Rigaku ATXG Thin Film diffractometer in slit-configuration with a Ni-filtered Cu source. Electrical measurements were performed with a Keithley 6430 subfemtoammeter and a Keithley 2400 source meter in ambient atmosphere or in a vacuum probe station at 10^{-6} Torr, as described previously [5c,11a,21]. Care was taken to protect the OFETs from ambient light prior to and during electrical measurements.

Received: September 10, 2007
Revised: November 21, 2007
Published online: April 9, 2008

[1] a) M. Chabinyc, Y.-L. Loo, *J. Macromol. Sci. Polym. Rev.* **2006**, *46*, 1. b) C. D. Dimitrakopoulos, P. R. L. Malenfant, *Adv. Mater.* **2002**, *14*, 99. c) C. D. Dimitrakopoulos, D. J. Mascaro, *IBM J. Res. Dev.* **2001**, 45. d) A. Dodabalapur, *Nature* **2005**, *434*, 151. e) A. Facchetti, *Mater. Today* **2007**, *10*, 28. f) G. Horowitz, *Adv. Mater.* **1998**, *10*, 365. g) G. Horowitz, *J. Mater. Res.* **2004**, *19*, 1946. h) H. E. Katz, Z. Bao, *J. Phys.*

Chem. B **2000**, *104*, 671. i) H. Sirringhaus, *Adv. Mater.* **2005**, *17*, 2411. j) Y. Sun, Y. Liu, D. Zhu, *J. Mater. Chem.* **2005**, *15*, 53. k) F. Würthner, *Angew. Chem. Int. Ed.* **2001**, *40*, 1037. l) C. R. Newman, C. D. Frisbie, D. A. da silva Filho, J.-L. Brédas, P. C. Ewbank, K. R. Mann, *Chem. Mater.* **2004**, *16*, 4436. m) Z. Bao, *Adv. Mater.* **2000**, *12*, 227. n) J. Zaumseil, H. Sirringhaus, *Chem. Rev.* **2007**, *107*, 1296.

[2] a) E. Da Como, M. A. Loi, M. Murgia, R. Zamboni, M. Muccini, *J. Am. Chem. Soc.* **2006**, *128*, 4277. b) M. A. Loi, E. Da Como, F. Dinelli, M. Murgia, R. Zamboni, F. Biscarni, M. Muccini, *Nat. Mater.* **2005**, *4*, 81.

[3] a) B. Yoo, T. Jung, D. Basu, A. Dodabalapur, B. A. Jones, A. Facchetti, M. R. Wasielewski, T. J. Marks, *Appl. Phys. Lett.* **2006**, *88*, 082104. b) B. Yoo, A. Madgavkar, B. A. Jones, S. Nadkarni, A. Facchetti, D. Dimmler, M. R. Wasielewski, T. J. Marks, A. Dodabalapur, *IEEE Electron Device Lett.* **2006**, *27*, 737. c) S.-H. Hur, M.-H. Yoon, A. Gaur, M. Shim, A. Facchetti, T. J. Marks, J. A. Rogers, *J. Am. Chem. Soc.* **2005**, *127*, 13808. d) H. Klauk, M. Halik, U. Zschieschang, F. Eder, D. Rohde, G. Schmid, C. Dehm, *IEEE Trans. Electron Devices* **2005**, *52*, 618.

[4] a) H. Klauk, U. Zschieschang, J. Pflaum, M. Halik, *Nature* **2007**, *445*, 745. b) S. De Vusser, S. Steudel, K. Myny, J. Genoe, P. Heremans, *Appl. Phys. Lett.* **2006**, *88*, 162116. c) K. Hizu, T. Sekitani, T. Someya, M. Otsuki, *Appl. Phys. Lett.* **2007**, *90*, 093504.

[5] a) B. Yoo, B. A. Jones, D. Basu, D. Fine, T. Jung, S. Mohapatra, A. Facchetti, K. Dimmler, M. R. Wasielewski, T. J. Marks, A. Dodabalapur, *Adv. Mater.* **2007**, *19*, 4028. b) Z. Bao, A. J. Lovinger, J. Brown, *J. Am. Chem. Soc.* **1998**, *120*, 207. c) B. A. Jones, M. J. Ahrens, M.-H. Yoon, A. Facchetti, T. J. Marks, M. R. Wasielewski, *Angew. Chem. Int. Ed.* **2004**, *43*, 6363. d) B. A. Jones, A. Facchetti, T. J. Marks, M. R. Wasielewski, *Chem. Mater.* **2007**, *19*, 2703. e) T. Jung, B. Yoo, L. Wang, B. A. Jones, A. Facchetti, M. R. Wasielewski, T. J. Marks, A. Dodabalapur, *Appl. Phys. Lett.* **2006**, *88*, 183102. f) B. A. Jones, A. Facchetti, M. R. Wasielewski, T. J. Marks, *J. Am. Chem. Soc.* **2007**, *129*, 15259.

[6] a) R. J. Chesterfield, J. C. McKeen, C. R. Newman, P. C. Ewbank, D. A. da silva Filho, J.-L. Brédas, L. L. Miller, K. R. Mann, C. D. Frisbie, *J. Phys. Chem. B* **2004**, *108*, 19281. b) R. J. Chesterfield, J. C. McKeen, C. R. Newman, C. D. Frisbie, *J. Appl. Phys.* **2004**, *95*, 6396. c) P. R. L. Malenfant, C. D. Dimitrakopoulos, J. D. Gelorme, L. L. Kosbar, T. O. Graham, A. Curioni, W. Andreoni, *Appl. Phys. Lett.* **2002**, *80*, 2517.

[7] A. C. Dürr, B. Nickel, V. Sharma, U. Täffner, H. Dosch, *Thin Solid Films* **2006**, *503*, 127.

[8] a) K. P. Pernstich, C. Goldmann, C. Krellner, D. Oberhoff, D. J. Gundlach, B. Batlogg, *Synth. Met.* **2004**, *146*, 325. b) J. Takeya, T. Nishikawa, T. Takenobu, S. Kobyashi, Y. Iwasa, T. Mitani, C. Goldmann, C. Krellner, B. Batlogg, *Appl. Phys. Lett.* **2004**, *85*, 5078. c) S. Kobayashi, T. Nishikawa, T. Takenobu, S. Mori, T. Shimoda, T. Mitani, H. Shimotani, N. Yoshimoto, S. Ogawa, Y. Iwasa, *Nat. Mater.* **2004**, *3*, 317.

[9] L.-L. Chua, J. Zaumseil, J.-F. Chang, E. C.-W. Ou, P. K.-H. Ho, H. Sirringhaus, R. H. Friend, *Nature* **2005**, *434*, 194.

[10] K. P. Pernstich, S. Haas, D. Oberhoff, C. Goldmann, D. J. Gundlach, B. Batlogg, A. N. Rashid, G. Schitter, *J. Appl. Phys.* **2004**, *96*, 6431.

[11] a) M.-H. Yoon, C. Kim, A. Facchetti, T. J. Marks, *J. Am. Chem. Soc.* **2006**, *128*, 12851. b) C. Kim, A. Facchetti, T. J. Marks, *Science* **2007**, *318*, 76.

[12] a) F. Würthner, *Chem. Commun.* **2004**, 1564. b) G. Klebe, F. Graser, E. Hadicke, J. Berndt, *Acta Crystallogr. Sect. B* **1989**, *45*, 69. c) Y. Che, A. Datar, K. Balakrishnan, L. Zang, *J. Am. Chem. Soc.* **2007**, *129*, 7234. d) H.-Z. Chen, M.-M. Shi, T. Aernouts, M. Wang, G. Borghs, P. Heremans, *Sol. Energy Mater. Solar Cells* **2005**, *87*, 521. e) Z. Chen, U. Baumeister, C. Tschierski, F. Würthner, *Chem. Eur. J.* **2007**, *13*, 450. f) A. Datar, R. Oitker, L. Zang, *Chem. Commun.* **2006**, 1649. g) M. G. Debije, Z. Chen, J. Piris, R. B. Neder, M. M. Watson, K. Müllen, F. Würthner, *J. Mater. Chem.* **2005**, *15*, 1270. h) X. Li, L. E. Sinks, B. Rybtchinski, M. R. Wasielewski, *J. Am. Chem. Soc.* **2004**, *126*, 10810. i) F. Nolde, W. Pisula, S. Mueller, C. Kohl, K. Müllen, *Chem. Mater.* **2006**, *18*, 3715. j) B. Rybtchinski, L. E. Sinks, M. R. Wasielewski, *J. Am. Chem. Soc.* **2004**, *126*, 12268. k) L. E. Sinks, B. Rybtchinski, M. Iimura, B. A. Jones, A. J. Goshe, X. Zuo, D. M. Tiede, X. Li, M. R. Wasielewski, *Chem. Mater.* **2005**, *17*, 6295. l) C. W. Struijk, A. B. Sieval, J. E. J. Dakhorst, M. van Dijk, P. Kimkes, R. B. M. Koehorst, H. Donker, T. J. Schaafsma, S. J. Picken, A. M. van de Craats, J. M. Warman, H. Zuilhof, E. J. R. Sudhölter, *J. Am. Chem. Soc.* **2000**, *122*, 11057. m) M. J. Tauber, R. F. Kelley, J. M. Giaimo, B. Rybtchinski, M. R. Wasielewski, *J. Am. Chem. Soc.* **2006**, *128*, 1782. n) T. van der Boom, G. Evmenenko, P. Dutta, M. R. Wasielewski, *Chem. Mater.* **2003**, *15*, 4068. o) T. van der Boom, R. T. Hayes, Y. Zhao, P. J. Bushard, E. A. Weiss, M. R. Wasielewski, *J. Am. Chem. Soc.* **2002**, *124*, 9582. p) X. Zhang, Z. Chen, F. Würthner, *J. Am. Chem. Soc.* **2007**, *129*, 4886. q) M. J. Ahrens, L. E. Sinks, B. Rybtchinski, W. Liu, B. A. Jones, J. M. Giaimo, A. V. Gusev, A. J. Goshe, D. M. Tiede, M. R. Wasielewski, *J. Am. Chem. Soc.* **2004**, *126*, 8284.

[13] M. Kasha, H. R. Rawls, M. A. El-Bayoumi, *Pure Appl. Chem.* **1965**, *11*, 371.

[14] a) J. Seibt, V. Dehm, F. Würthner, E. Volker, *J. Chem. Phys.* **2007**, *126*, 164308. b) J. Seibt, P. Marquetand, V. Engel, Z. Chen, V. Dehm, F. Würthner, *Chem. Phys.* **2006**, *328*, 354. c) F. Spano, *J. Chem. Phys.* **2005**, *122*, 234701.

[15] A. J. Mäkinen, A. R. Melnyk, S. Schoemann, R. L. Headrick, Y. Gao, *Phys. Rev. B* **1999**, *60*, 14683.

[16] a) A. B. Chwang, C. D. Frisbie, *J. Appl. Phys.* **2001**, *90*, 1342. b) T. W. Kelley, C. D. Frisbie, *J. Phys. Chem. B* **2001**, *105*, 4538.

[17] S. E. Fritz, T. W. Kelley, C. D. Frisbie, *J. Phys. Chem. B* **2005**, *109*, 10574.

[18] E. Hadicke, F. Graser, *Acta Crystallogr. Sect. C* **1986**, *42*, 189.

[19] J. G. Laquindanum, H. E. Katz, A. Dodabalapur, A. J. Lovinger, *J. Am. Chem. Soc.* **1996**, *118*, 11331.

[20] M. J. Ahrens, M. J. Fuller, M. R. Wasielewski, *Chem. Mater.* **2003**, *15*, 2684.

[21] a) A. Facchetti, G. Hutchison, M.-H. Yoon, J. Letizia, M. A. Ratner, T. J. Marks, *Polym. Prepr. Am. Chem. Soc. Div. Polym. Chem.* **2004**, *45*, 185. b) A. Facchetti, J. Letizia, M.-H. Yoon, M. Mushrush, H. E. Katz, T. J. Marks, *Chem. Mater.* **2004**, *16*, 4715. c) A. Facchetti, M. Mushrush, M.-H. Yoon, G. R. Hutchison, M. A. Ratner, T. J. Marks, *J. Am. Chem. Soc.* **2004**, *126*, 13859. d) A. Facchetti, M.-H. Yoon, C. L. Stern, H. E. Katz, T. J. Marks, *Angew. Chem. Int. Ed.* **2003**, *42*, 3900. e) J. A. Letizia, A. Facchetti, C. L. Stern, M. A. Ratner, T. J. Marks, *J. Am. Chem. Soc.* **2005**, *127*, 13476. f) M.-H. Yoon, S. DiBenedetto, A. Facchetti, T. J. Marks, *J. Am. Chem. Soc.* **2005**, *127*, 1348.